Space Weather Effect via Periodic Photometric Observations of Geostationary Satellites

Matej Zigo
Comenius University in Bratislava, Slovakia
Katarína Sabolová
Comenius University in Bratislava, Slovakia

Jiří Šilha
Comenius University in Bratislava, Slovakia

ABSTRACT

Space weathering affects all objects exposed to the environment of space – including artificial satellites – causing optically detectable deterioration of surface materials. Space weathering includes a combination of effects, such as solar high-energy particles, micrometeoroid impacts, and – at lower altitudes – atmospheric particles interacting with the object's surface. As previously indicated by laboratory tests, space weathering of artificial materials exhibits rapid changes during the initial months in orbit [1]. Subsequently, the materials undergo a period of stabilization, and the observed changes are less pronounced. The visible changes to the surface properties of artificial satellites can be measured by annual observations using BVRcIc photometric passbands. Based on laboratory simulations under similar conditions, the overall reflectance of the surface decreases – darkens – but it does so dependently on material type and wavelength, darkening greatly in shorter (blue) wavelengths and only moderately in longer (red) wavelengths – giving the impression of reddening of the surface. This subsequently affects the color indices $(B–V)$ differently than $(R_c–I_c)$. Furthermore, such behavior in $(B-V)$, $(R_c–I_c)$ and $(B–I_c)$ can be directly translated into spectral interpretation, to increase the amount of data available for object characterization. As the color indices vary with phase angle and orientation, observations must be conducted regularly during the same time of year and with regards to the object's rotational period. Observation of functional geosynchronous satellites proves convenient, as operating GEO satellites are generally non-rotating objects. Regularly collected photometric data were acquired over the course of five years by the 70 cm Newtonian telescope AGO70, operated by Comenius University in Bratislava, Slovakia under the nominal color photometry program [2]. Over ten GEO satellites – launches between 2006 and 2015 – were observed since 2019, during the months of July and August. Annual GEO satellite color indices and their change over time will be presented with regards to their dominant surface material type, bus architecture groups, and possible causes through the comparison with laboratory acquired data will be discussed.

[1] Engelhart, D. P., Cooper, R., Cowardin, H., Maxwell, J., Plis, E., Ferguson, D., ... & Hoffmann, R. (2019). Space weathering experiments on spacecraft materials. The Journal of the Astronautical Sciences, 66(2), 210-223. [2] ZIGO, Matej, et al. Space debris surface characterization through BVRcIc photometry. Advances in Space Research, 2023, 72.9: 3802-3817.

1. INTRODUCTION

Space weathering and aging refer to the physical and material changes that occur on the surfaces of airless bodies such as asteroids, comets, and artificial satellites, due to prolonged exposure to space environments. These effects were initially described in the study of asteroid compositions and the definition of taxonomy groups [1].

Space weathering involves surface alteration due to solar wind particles, micrometeoroid impacts, and cosmic rays, leading to darkening, changes in reflectance properties, and mineralogy. This can make identifying the original composition difficult, as seen in the formation of regolith on asteroid surfaces [2]. Aging effects, on the other hand, encompass the cumulative surface changes over time, such as the accumulation of weathering products, rock breakdown, and crater formation.

These effects impact the interpretation of spectroscopic and photometric data, making it harder to determine the mineralogy of these bodies accurately [5]. For artificial materials, space weathering and aging can cause corrosion, cracking, paint degradation, and other structural compromises that threaten spacecraft durability. Therefore, understanding these effects on different time scales is crucial for extending mission lifespans.

Unlike natural bodies, space debris experiences shorter exposure to the space environment, ranging from 0 to 30 years, compared to millions of years for asteroids. This study focuses on artificial objects, particularly space debris, using operational satellites to draw conclusions on material aging. The space debris population includes all non-functional artificial objects in orbit, such as spent rocket bodies, upper stages, and fragments from collisions. Public catalogs track over 28,000 objects larger than 10 cm using radar and optical techniques [9], [10].

Space weathering and aging effects have been studied in laboratory conditions as well. For instance, [4] simulated space conditions to examine changes in Kapton and Mylar Multi-Layer Insulation (MLI) foils exposed to high-energy electrons in the GEO region. This led to visible darkening and spectral reddening in the first years on orbit. Kapton, typically transparent between $500-700$ nm, saw a shift in absorption toward 730 nm, due to chemical damage from electron bombardment [3].

The extent of weathering is highly material-dependent. While insulation foils redden, white paints often shift toward bluer hues [6]. Laboratory tests suggest that initial reflectivity decreases, especially in the blue part of the spectrum, differ from changes in the red part. Unlike MLI materials, white paint on upper stages showed greater decreases in the red spectrum, resulting in a bluing effect.

In our study, we use standard color photometry (BVR_cI_c) based on Johnson/Cousins filters to measure object brightness. This paper presents the results of a long-term monitoring campaign targeting geostationary orbits. Over four years of color observations, we estimate linear color change rates to test hypotheses drawn from laboratory studies on space weathering and aging effects.

1.1 Instrumentation

All data used for our research are originated in the 70 centimeter aperture newtonian reflector (AGO70) (see Figure 1 and Table 1). It is situated around 30 km far from the Bratislava at the Astronomical and Geophysical observatory in Modra, Slovakia (AGO) of Comenius University and registered at Minor Planet Center observatory list with code M34 ([7]). The location of the AGO is at latitude N 17.274 degrees, longitude E 48.373 degrees and altitude of 536.1 meters above the see level. This computerized scientific instrument is operated by the Faculty of Mathematics, Physics and Informatics (FMPH), Comenius University, Bratislava.

Fig. 1: The AGO70 newton telescope on fork equatorial mount. Credit: Stanislav Griguš

1.2 Campaign

As discussed in the Introduction section, based on the laboratory measurements of the spaceweathering and aging effects, general hypothesis for the commonly used materials as MLIs or solar panels, the reddening effect might occur on the surfaces of the artificial satellites.

We selected several operational geostationary satellites as test targets for our hypothesis, primarily because they remain in the same position in the sky year-round. This simplifies observation as no advanced tracking methods are required,

Table 1: AGO70 definition parameters. Credit: [8]

Operator	FMPH		
Telescope	AGO70		
Telescope design	Newton		
Mount	Equatorial (Open fork)		
Camera CCD	FLI-ProLine KAF-1001E		
Dimension	1024x1024		
Camera peak efficiency	±72% at 565 nm		
Camera sensitivity interval	300 nm - 1060 nm		
Primary Mirror [mm]	700		
Focal length [mm]	2962.0		
Focal ratio	f/4.2		
FoV [arc-min]	28.5 x 28.5		
iFoV [arc-sec/px]	1.6		
Photometric filters	Type	λ_{eff}	FWHM
	B	435.9 nm	88.4 nm
	V	545.6 nm	83.7 nm
	R_c	654.8 nm	138.9 nm
	I_c	789.2 nm	150.1 nm

and their near-zero angular velocities allow for longer exposure times, improving the signal-to-noise ratio and data accuracy. Additionally, we focused on operational satellites, as their attitude is stabilized and directed at a specific Earth region, ensuring the same side is observed during each session.

After applying these criteria, the phase angle (Sun-target-observer) remained the only variable in the observational geometry. To account for this, we took at least three measurements per observation session—before opposition (approximately 45°), near opposition (within ±10°), and after opposition (approximately 45°). These measurements were averaged to minimize the phase angle's impact. Each measurement point was collected in under 5 minutes to ensure the phase angle changed by no more than 3°, meeting our internal requirement.

The long-term monitoring campaign began in 2019 and continued until the summer of 2023. Observations were conducted monthly, only on nights with stable weather and around the new moon to avoid interference from clouds and moonlight. As an example for this study we selected from our target list the Astra cluster i.e., satellites Astra 1M (NORAD 33436), Astra 1N (NORAD 37775), Astra 1KR (NORAD 29055) and Astra 1L (NORAD 31306) as show in the Table 2.

Table 2: Table of selected attitude stabilized satellites situated on GEO ring. Showed are COSPAR designator, NORAD number, ID of the used platform and age at the start of the campaign at 2019.

Name	**COSPAR**	**NORAD**	**Platform**	**Age**
ASTRA 1N	2011-041A	37775	Eurostar-3000	8 years
ASTRA 1L	2007-016A	31306	LM A2100	12 years
ASTRA 1KR	2006-012A	29055	LM A2100	13 years
ASTRA 1M	2008-057A	33436	Eurostar-3000	11 years

2. RESULTS

For each observation night we calculated the nightly standard color indices for each satellites. These values has been then summarized and averaged into the annual color indices which are reported in this section. The nominal data quality is defined by the input data conditions, which requires, that no data with Signal-To-Noise Ratio (SNR) bellow 30, can be processed. Therefore, the nominal data quality in terms of magnitudes is ±0.03mag.

Data processing starts with the light curve estimation and data conversion into the standard system of magnitudes. Overall process follows the methods of the photometric reduction discussed and defined in [11].

Based on the age (more than 8 years at start of the campaign) of the selected targets we do not anticipate to see very fast reflectivity and color changes, which nominally occur in the beginning of the satellite's lifetime [4]. Therefore, once the annual color indices are extracted, we optimize the general trend in the measurements by linear function to estimate the general slope of the trend line, which corresponds to the annual color change rate. Such estimation is done in three different color indices: $(B-V)$ - representing the shorter wavelengths i.e., blue colors; (R_c-I_c) - representing the longer wavelengths i.e., red colors; $(B-I_c)$ - representing the color indices containing two most distinct passbands available on our system i.e., summarizing the changes of the overall reflectivity changes in the visible spectrum.

The result for the Astra cluster satellites can be seen on Figures 2,3,4,5 and in the color rates are reported in the Table 3.

Based on these measurements can be seen that for each Astra satellite, we measure positive color index rates at each extracted channel. The nominal annual color rates are in the interval from 0.01 mag/year up to 0.06 mag/year in $(B-V)$ and (R_c-I_c) and more than 0.1 in $(B-I_c)$. For each target we measure slightly higher color index rates for the $(B-V)$ in the comparison to the (R_c-I_c). Furthermore, the positive $(B-I_c)$ rate was measured for each target. These two results can be directly interpreted as reddening of the surface materials, as the reflectivity must decrease faster in the shorter wavelengths as in the longer wavelengths to be able to generate such color rates.

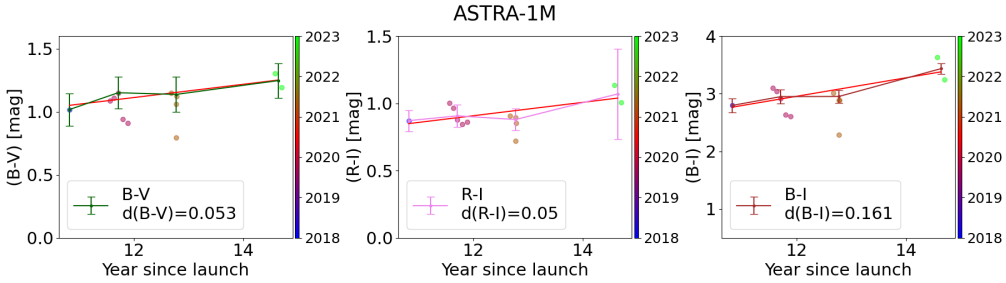

Fig. 2: Evolution of the color indices $(B-V)$, $(R-I)$ and $(B-I)$ for Astra 1M (NORAD 33436). Plotted are nominal acquired nightly color indices, median annual color index and linear trend of the color index changes. In the legends are shown also the color index linear rates *dCI*.

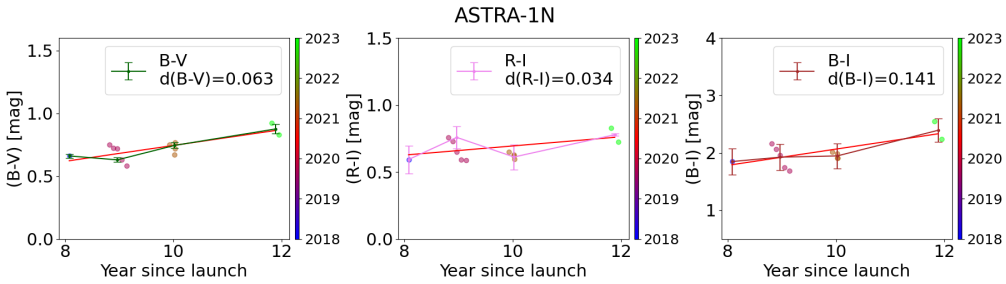

Fig. 3: Evolution of the color indices $(B-V)$, $(R-I)$ and $(B-I)$ for Astra 1N (NORAD 37775). Plotted are nominal acquired nightly color indices, median annual color index and linear trend of the color index changes. In the legends are shown also the color index linear rates *dCI*.

3. DISCUSSION AND CONCLUSION

Our findings fully validate the reddening hypothesis and demonstrate that color photometry is a valuable tool for assessing satellite health and platform aging. With more precise data and material properties from laboratory studies, it could be possible to deconvolve the reflected light and identify which materials are most affected by degradation. This approach holds promise for identifying satellite vulnerabilities and potentially extending their operational lifespans.

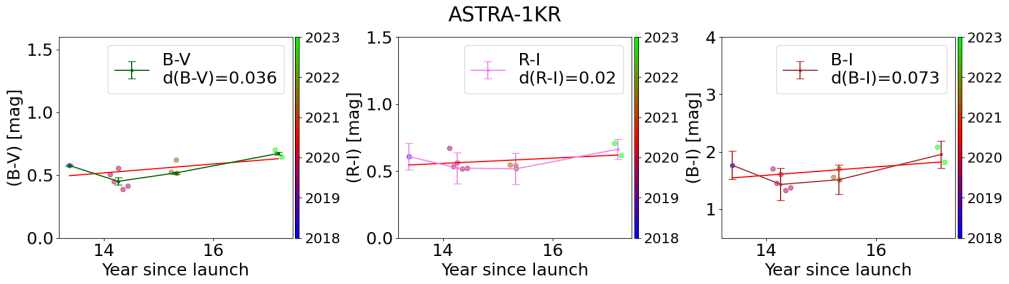

Fig. 4: Evolution of the color indices $(B-V)$, $(R-I)$ and $(B-I)$ for Astra 1KR (NORAD 29055). Plotted are nominal acquired nightly color indices, median annual color index and linear trend of the color index changes. In the legends are shown also the color index linear rates *dCI*.

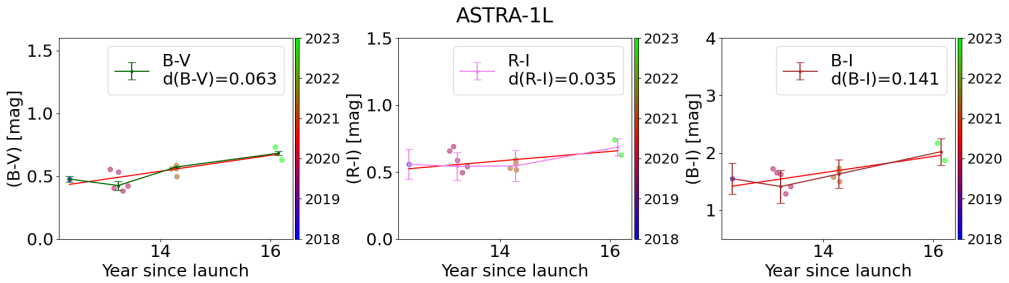

Fig. 5: Evolution of the color indices $(B-V)$, $(R-I)$ and $(B-I)$ for Astra 1L (NORAD 31306). Plotted are nominal acquired nightly color indices, median annual color index and linear trend of the color index changes. In the legends are shown also the color index linear rates *dCI*.

FMPH and AGO70 will continue to monitor geostationary satellites and plan to expand the target list to cover more platforms and missions. Currently, we are analyzing linear trends in the data to estimate the nature of color shifts. However, future efforts will focus on applying specific physical models of satellite aging to better understand the causes of these variations.

For all observed targets, we identified a general trend in the evolution of the color index, especially through the $(B-I)$ color index, which highlights shifts in the most distant passbands, indicating whether the spectrum shifts toward red or blue. Our measurements show that all observed satellites lose reflectivity more rapidly at shorter wavelengths, confirming the reddening effect. This conclusion is reinforced by the color rates in the $(B-V)$ and $(R-I)$ indices.

It is important to note, however, that the reported color rates cannot be directly attributed to specific materials, as the measurements reflect the combined light from various satellite surfaces, including solar panels, payloads, and structural components. Furthermore, due to the photometric limitations at the AGO70 site—stemming from low elevation, urban proximity, and uncertainty in the extinction coefficient—we are unable to perform a more detailed deconvolution of the satellite's reflection.

Table 3: Color index rates for all measured targets during the campaign.

Name	d(B-V)	d(R-I)	d(B-I)
Unit	[mag/year]	[mag/year]	[mag/year]
ASTRA-1M	0.053	0.050	0.161
ASTRA-1N	0.063	0.034	0.141
ASTRA-1KR	0.036	0.020	0.073
ASTRA-1L	0.063	0.035	0.141

4. REFERENCES

[1] Clark R. Chapman. S-type asteroids, ordinary chondrites, and space weathering: The evidence from galileo's fly-bys of gaspra and ida. *Meteoritics & Planetary Science*, 31(6):699–725, 1996.

[2] B. E. Clark, B. Hapke, C. M. Pieters, and D. Britt. Asteroid space weathering and regolith evolution. *Asteroids III*, pages 585–599, 2002.

[3] D. P. Engelhart, E. Plis, S. Humagain, S. Greenbaum, et al. Chemical and electrical dynamics of polyimide film damaged by electron radiation. *IEEE Transactions on Plasma Science*, 45(9):2573–2577, 2017.

[4] D.P. Engelhart, R. Cooper, H. Cowardin, J. Maxwell, et al. Space weathering experiments on spacecraft materials. *The Journal of the Astronautical Sciences*, 66(2):210–223, 2019.

[5] M. J. Gaffey. Space weathering and the interpretation of asteroid reflectance spectra. *Icarus*, 209(2):564–574, 2010.

[6] R. Hoffmann, R. Cooper, S. Schieffer, D. Ferguson, et al. Optical characterization of commonly used thermal control paints in a simulated geo environment miles bengtson, jordan maxwell university of colorado boulder. In *Advanced Maui Optical and Space Surveillance (AMOS) Technologies Conference*, 2018.

[7] IAU Minor Planet Center. Minor Planet Center - observatory list. `https://minorplanetcenter.net/iau/lists/ObsCodesF.html`, 2023. Online; Accessed: 24.02.2023.

[8] J. Šilha, S. Krajčovič, M. Zigo, J. Tóth, et al. Space debris observations with the Slovak AGO70 telescope: Astrometry and light curves. *Advances in Space Research*, 2020.

[9] SpaceTrack. Spacetrack. `https://www.space-track.org`, 2024. Online; Accessed: 01.08.2024.

[10] D. Vallado, P. Crawford, R. Hujsak, and T. S. Kelso. Revisiting spacetrack report# 3. In *AIAA/AAS Astrodynamics Specialist Conference and Exhibit*, page 6753, 2006.

[11] Matej Zigo, Jiří Šilha, Tomáš Hrobár, and Peter Jevčák. Space debris surface characterization through bvrcic photometry. *Advances in Space Research*, 72(9):3802–3817, 2023.